International Journal of Energetica (IJECA)
https://www.ijeca.info
ISSN: 2543-3717 Volume 8. Issue 2. 2023
Page 44-53

Principal Component Analysis-Based Shading Defect Identification and Categorization in Standalone PV Systems Using I-V Curves

Hayder Dakhil Atiyah[1*], Mohamed Boukattaya [2], Fatma Ben Salem [3]

[1]Department electrical power at National School of Engineering of Sfax, TUNISIA
[2] Laboratory of sciences and Techniques of Automatic Control & Computer Engineering (Lab-STA), ENIS Sfax, TUNISIA
[3]Control and Energy Management Laboratory (CEMLab), ENIS Sfax University, TUNISIA

[*]Corresponding author E-mail: haydergfg@gmail.com

Abstract – *Photovoltaic (PV) system health monitoring and fault diagnosis are essential for optimizing power generation, enhancing reliability, and prolonging the lifespan of PV power plants. Shading, especially in PV systems, leads to unique voltage-current (I-V) characteristics, serving as indicators of system health. This paper presents a cost-effective and highly accurate method for detecting, diagnosing, and classifying shading faults based on real I-V data obtained through electrical measurements under both healthy and shaded conditions. The method leverages Principal Component Analysis (PCA) to separate classes, and a confusion matrix assesses classification accuracy. The results demonstrate a success rate exceeding 98% in various configurations, using experimental data from a 250 W PV module. Importantly, this method relies solely on existing electrical measurements, eliminating the need for additional sensors, making it both efficient and cost-effective.*

Keywords: Pv model, Principal component analysis, Health system, temperature, irradiation

Received: 14/10/2023 – Revised: 09/11/2023– Accepted: 12/12/2023

I. Introduction

Due to advances in PV installation technology and the increasing demand for sustainable energy in various applications (satellites, telecommunication, electric vehicles, residences, agriculture), PV systems have gained significant interest. With a global installed power of 402 GW by the end of 2022, solar PV now ranks as the third-largest renewable energy source, surpassing hydro and wind [1]. Solar power system efficiency is typically capped at 15% to 20%. A study [2] found that PV modules show an annual performance deterioration rate of 0.924% [3], and a recent study reported a 1.55% yearly rate of maximum output deterioration with the same PV technology. PV systems can develop a number of different defects. Many variables, including material interactions (damage of connectors, change color and discoloration of the material for encapsulating, as well as (discoloration of busbars.) and environmental conditions, for instance, soiling and shadowing, may contribute to these flaws. PV panels can get "soiled" with debris like snow, dirt, leaves, and bird droppings [4]. Shading, caused by obstacles like chimneys and trees, is a common issue during operation, significantly reducing PV system performance. Research by Decline et al. found that partial shadowing can lead to a 10–20% annual drop in power production in residential applications (2011). Even with bypass diodes, localized shadowing can cause shaded cells to overheat, evidenced by hot spot regions in infrared thermography studies [1]. As a result, a temperature rise in these areas causes a power loss [2] significantly shortens the lifetime of the PV units, and potentially harms the cells in shade [3]. For obvious safety and financial reasons, the detection of such suboptimal operating circumstances has become essential. Frequently, developing the diagnostic process demands considerable equipment or incurs high costs. The three fundamental methods for diagnosing PV faults

are generally data-driven, relying on various diagnosis techniques. These techniques are gaining popularity due to their effectiveness in accurately isolating faults and efficiently detecting their presence within a PV plant. Optical inspection methods, requiring expensive specialized tools such as heat cameras and silicon charged coupled device (CCD) cameras, are known for their high accuracy. Electroluminescence (EL)-based diagnosis techniques effectively identify issues like Position of Interaction Failures (PIF), Cell damage and Shunts (CDS), Unoccupied PV Cells or Substrings (caused by sudden cutoff or shunted in the Bypass Diodes connection), and potential static-induced deterioration (PID). However, this method requires specific test conditions, including the use of a high pass filter and a high-resolution camera. Electroluminescent inspections must be conducted beyond the maximum power point (MPP) or after the PV system has been stopped to promote radiations restructuring in the PV cells, necessitating the system to be driven by a DC current. Consequently, experimental design becomes challenging, expensive, and costly, particularly for large PV systems. This method is more suitable for tiny PV systems. Infrared thermography (IRT) measurements are used both inside and outside the MPP operation. Flaws detected using IRT are comparable to those discovered with electroluminescence (EL) imaging and significantly affect the thermal behavior of flawed PV modules. The IRT-based technique quickly and precisely locates problems without interrupting the functioning of the PV system. However, IRT also requires specific conditions such as clear, bright sunshine with high irradiation, low outside temperatures, minimal wind, and precise viewing angles to accurately measure temperature. Model-based methods often employ PV analytical models to calculate parameters, allowing for a comparison with measured data. The residues produced are used for diagnostics as defect characteristics. Recently, some model-based methods derive conclusions from the analysis of solar cell power losses. These models require irradiance and PV generator temperature data to estimate the PV system's power output [9]. Emerging model approaches utilize empirical criteria (short-circuit current, fill factor, open-circuit voltage, etc.) determined by the geometry of the I-V curves for current-voltage [10]. Many studies on PV monitoring and diagnosis now exist, but they depend on the employed model and the operation's time period [11]. Infrared thermography (IRT) and Electroluminescence (EL) imaging, under steady-state conditions, are common image-based PV techniques due to their minimal hardware requirements and versatility with various PV systems [11]. These techniques are effective for detecting shading in a system. Data-based strategies rely on operationally collected historical data, retrieving and analyzing fault characteristics for defect diagnosis, using signal processing, machine learning, and computational intelligence [12]. Some signal processing techniques, particularly in the time domain, are applied to detect ground-fault, catastrophic faults, and PV arc faults [14]. Methods that extrapolate PV module defect characteristics or analyze the I-V metrics of strings or arrays are used to determine shading issues [15]. By analyzing the first and second order derivatives of I&V curves, these techniques determine if the activation of bypass diodes hints at a shading problem during both normal and shaded operations [16]. While quick and efficient at finding shading errors, they may not distinguish between different shading patterns [17]. Intelligent networks (ANN) and fuzzy logic classifiers are popular techniques for detecting shading faults [18]. However, their drawbacks include sensitivity to imbalanced climatic circumstances, the need for a wide range of training data for accuracy, and a time-consuming training phase [19]. Additionally, the data gathered is specific to a particular PV installation, making the rules closely related to the system being studied [20]. Consequently, the rules are closely tied to the system under study [21]. Another drawback of these methods is the requirement for regular updates to the training data. This is necessary due to the wide variability in observed operating conditions, such as changes in climate or the degradation and aging of solar cells [22]. For instance, training data under decreased irradiance and temperature conditions may inaccurately categorize measurement data and lead to false alarms for healthy operational parameters when there's an increase in irradiance and temperature. However, a substantial amount of data can be collected for research by utilizing PV systems while in use [23]. Data-driven modeling is relevant, where features can be extracted and subsequently analyzed for defect diagnostics. Principal Components Analysis (PCA) is a widely used statistical method for data exemplification and categorization in these techniques for feature extraction [24]. PCA proves powerful for diagnostics, excelling in classification across various applications. It is particularly beneficial in complex systems where PCA hasn't been applied to study characteristics retrieved from authentic I&V curves. For PV modules, the suggested procedure involves using software like MATLAB and Minitab. The discussion on PCA's performance for fault classification and detection is based on achieved results, including the creation of a new implicit PCA model (FDC). This model stands out for its simplicity, minimal training costs, and accurate

data viewers, suitable for current PV installations. Integrated online I&V tracing allows FDC diagnostics for photovoltaic modules under various operating conditions.

In this study, we propose to examine the efficacy of a shading defect identification approach that can work with any connected PV system. Utilizing the existing measurements in these systems and requiring no additional hardware, the recommended strategy demonstrates strong classification capabilities for the same type of defect. Moreover, it exhibits the capacity to distinguish between healthy and flawed data, specifically in the context of shading. The PCA method employed in this approach effectively classifies various shaded arrangements.

II. Preliminary research: I&V curve analysis for various faults

Deterioration modes in PV systems are reflected in I-V curves, notably under low light conditions due to bypass diode activation. The PV module under standard test conditions (STC) shares specifications with this study, featuring a 0.3-ohm series resistance [25]. Fig. 1 illustrates simulation results showcasing the impact of specific PV faults under varying conditions: healthy state, shading, and increased series resistance. Shading results in erratic illumination in sub-strings, while reduced series resistance primarily affects the I-V curve near the open circuit voltage [26].

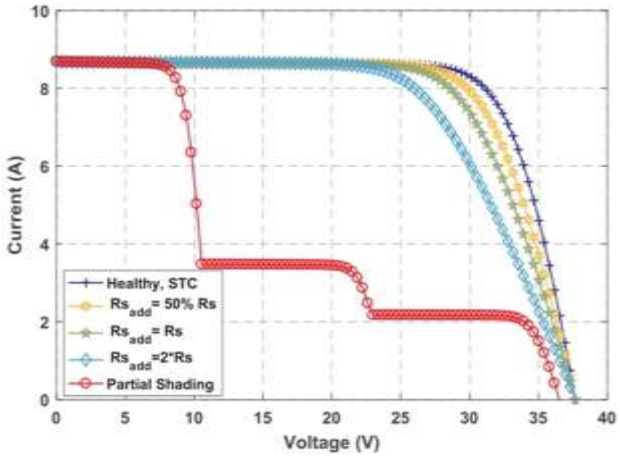

Figure 1. I-V curve's I-V fault signatures

Figure 2 shows the PCA outcomes in the subspace covered by PC1 and PC2 for the simulated PV faults.
The partial shading defect may be differentiated from the deteriorated series resistance, according to Figure 2, by projecting the data into a new reference frame enclosed by (PC1, PC2). However Further data processing or/and more information should be done or included to distinguish the healthy case from the degraded series resistance. We will concentrate on detecting shading faults using experimental data in these sections that follow. Also, more information about the features chosen for PCA evaluation will be given.

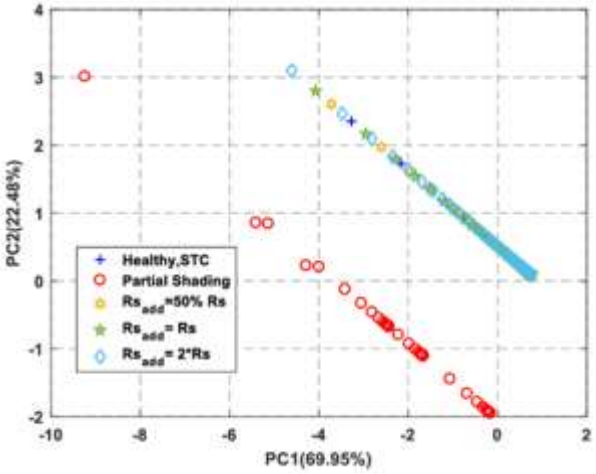

Figure **2**. PCA outcomes in the subspace covered by PC1 and PC2 for the simulated PV faults

III. PV systems shadowing situation

The standard electrical circuits that are consist of one or two equivalent diodes that are employed to replicate the I-V feature of a PV cell. In order to provide a better representation that is physical events in solar cell, other models have been devised. As the traditional single diode model accurately reproduces the key traits of a PV cell, it is frequently utilized. With these systems, shading of the entire or a portion of the PV, the system surface is a major worr. PV systems are fitted with bypass diodes to lessen the impact of shade. when solar power cells are shaded and biased in the reverse conditions, these diodes turn on. The shaded cells are short-circuited when these diodes are turned on, which reduces their reverse voltage and, in turn, the power dissipated. In actual use, one bypass diode is often wired across a collection of 18–20 cells.

3.1. Description of the experimental setup

The proposed fault detection method is evaluated using real data from a PV module as shown in Table 1, following STC parameters (1000 W/m^2/ 25 °C) [30]. The module comprises three substring combinations of 20 PV cells each connected in series with three bypass diodes for protection. I-V curves are generated with 3000 data points per curve, ranging from open-circuit voltage to short-circuit current, using a variable load. Various

methods, such as resistive loads and capacitors, can be employed for impedance variation based on PV power and measurement precision requirements. In this study, 3000 samples effectively cover the module's I-V curve.
Using a solar radiation meter scop, determine Figure 3. Shown the measurement of experimental from I&V curve three period when the PV system operation in healthy condition and clear result condition (greater than 850 W/m^2). While the current of short-circuit a PV experimental, experiments have been performed. They were realized under a variety of operating conditions. One healthful setting

The flawed modes under different shading circumstances: Changes in the PV cells' exposure to light result in the application of shade for each set. Data from the experiment is unnecessary. For each set of both. A healthy state MATLAB software, and the data consumption is confirmed and presented in detail by the schematic diagram displayed in Figure 3.

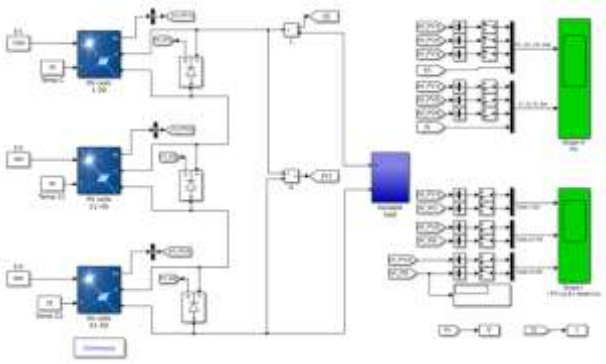

Figure. 3. Experimental setup layout using simulation of Matlab

3.2. Data gathering (Data question)

An evaluation of the fault detection approach involved four experimental sets. Experiments were conducted under a variety of operating conditions, including one healthful setting. The flawed modes were tested under different shading circumstances, simulating changes in the exposure of the PV cells to light for each set. Experimental data is deemed unnecessary for both sets.

3.2.1. A healthy state

Figure 4 Shown the measurement of experimental from I&V curve three period when the PV system operation in healthy condition and clear result condition (greater than 850 W/m^2). While the current of short-circuit a PV healthy and illogical test, we have recorded three measurements (A-mes, B-mes, and C-mes) of a whole I-V characteristic. A-mes and B-mes collected data sets will be used for the training stage, and C-mes as confirmation, as detailed under Section 4. I-V curves are made up of 3000 samples each. It is captured for a minute. For methodology to sweep an entire I-V characteristic's, 101 samples are sufficient in order to show the I-V curve's deviations and inflection points clearly, the number of samples indicated required to extractor these features it is often chosen based on the figure of the PV units and the Mismatched terms. Despite the close proximity of measurements, the irradiation can vary considerably. The three examples A-mes, B-mes, and C-mes are Depicts the details for each I & V curve (Figure 4) as blue color, red color, and mustard lines, respectively. module is related to sun irradiance; when exposed to low quantities of solar radiation, it produces less current. can note results are consistent according to datasheet information offered under STC (Table 1).

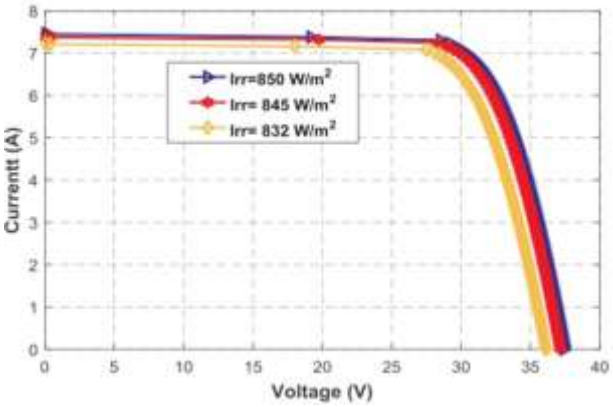

Figure 4. I-V experimental a healthy state of the curve

Table 1. STC's requirements for PV modules

Symbols of Quantities	Value
Pmpp Max Power	250 (W)
Impp Current at pmpp	8.22(A)
Vmpp Voltage at pmpp	30.51(V)
Isc Short-circuit Current	8.65 (A)
Voc Open-circuit voltage	37.66 (V)

3.2.2. Lighting conditions (shading)

Figure 5 shows the activation of diodes' I &V properties, measured three period for each arrangement, and the four shading configurations. All I-V curves in shaded situations exhibit different peaks that can be shown by the condition of the bypass diode in connection to the different kinds of shading that have been used. These peaks show how PV units lose efficiency when shaded because their maximum output power is reduced. Due to its partial shading, the PV cells in the test module receive uneven illumination. Take in mind that the sun irradiation listed in the caption to each I-V characteristic corresponds to the measurement made with the data of reference cell. The curves of experimental behavior changes depending on the variance of shading (row

measurements level, column measurement level, and shaded cells) and external factors (temperature and sun irradiation).

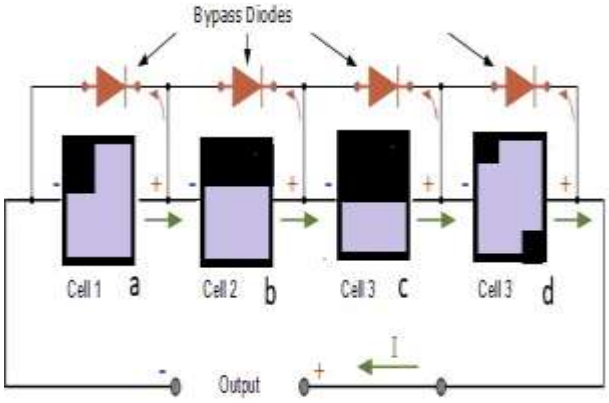

Figure 5. Activation of diodes' I &V properties

The first shading configuration, which is depicted in Fig. 5a, partially shades one PV sub-string. When 12 cells are shaded, one bypass diode is activated, which deactivates the problematic sub-string. The voltage sharp change caused by the loss of this sub-string serves as confirmation of this. (Fig. 5a), the remaining combinations trigger two bypass diodes since each configuration has two sub-strings that are partially shaded. Depending There are two scenarios depending on how severe the shading defect is: either all of the diodes are conducting simultaneously (Fig. 5a), in which case there is only one voltage maximum (Fig. 5c), or all of those diodes are flowing sequentially (Figs. 5b and d), in which case there are two voltage peaks.

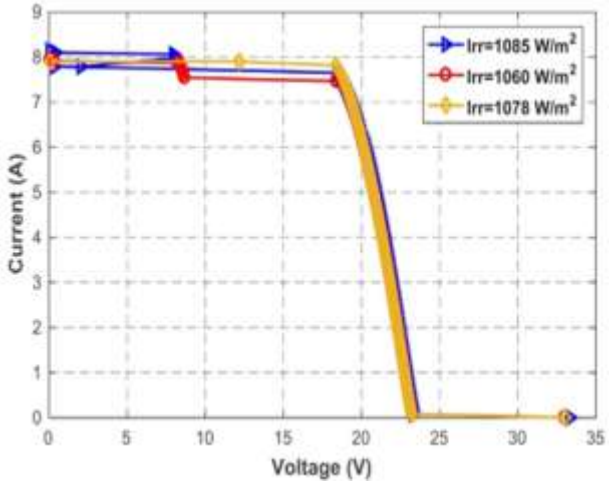

State (a)

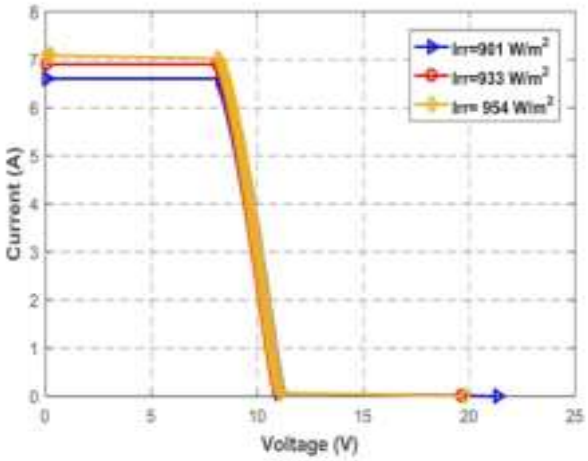

State (b)

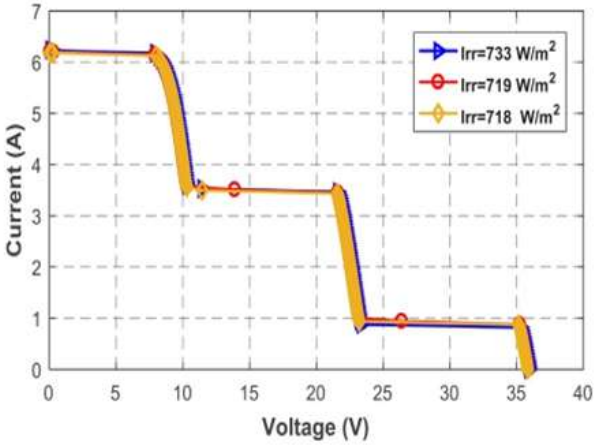

State (c)

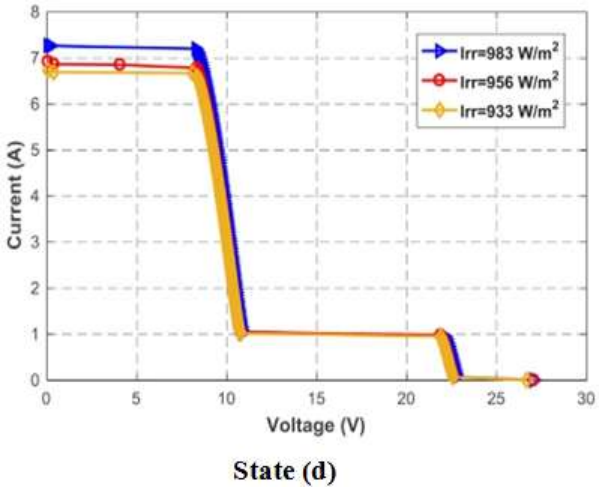

State (d)

Figure 5. Experimental I-V curves and the shading configurations (a) , (b), (c), and d

3.2.3. Reproducibility of data

The I&V curves three copies were obtained for each experimental testing. for our evaluation. Data

redundancy's main purpose for the diagnosis algorithms is to create a database. Training and test data will be separated from this database. The results of the experimental testing demonstrate that the shading errors significantly alter the I-V features form. Therefore, the paper proposal examines a usage of the cure of area as a metric to investigate the variable between the duplicated Data is collected through each pilot test. According to the PV voltage and current, it is calculated. We take into account the normalized current in relation to the observed irradiation. The following is how the AUC is approximated

$$AUC = \sum_{i}^{n} \frac{1}{2}\left[\left(v_j - v_{j-1}\right)\left(I_{norm\ .j} - I_{norm-1}\right)\right] + I_{norm.j-1}\left(v_j - v_{j-1}\right) \quad (1)$$

$$Inorm = I\ \frac{G_{STC}}{G_{mes}} \quad (2)$$

where GSTC and G_{mes} stand for the STC and measured irradiations, respectively. Table 2 provides the average and the AUC's relative inaccuracies obtained during each test. We can see right away that healthy conditions yield the highest AUC values. The I-V curves are in agreement with this. The primary variables in this region are the type of shading defect and a test circumstance (healthy of system or faulty system). The I-V values acquired for each test are extremely similar when the measurements are repeated, it agrees with the method of measuring for one minute. The sun's irradiance actually fluctuates very little, reaching a maximum rate of 14 W/m^2 in a healthy the case 25 W/m^2 in the first problematic configuration 51 W/M^2 in the second, 52 W/M^2 in the third, and 15 W/m2 in fourth. The largest relation error that can be determined for in a normal operation is 4.68%, while it is 2.37% in a dysfunctional one's. This deference leads us to make the assumption that the database may be utilized to assess fault detection and is representative of all operating situations.

- Detection of shading errors (under fault)

In Figure 6, the method's flowchart is visible. The modeling process is the first phase. The experimental results for the defect in all healthy PV shading scenarios are represented by 67% of the training data. The pre-processing of the data makes up the second step. The matrix X is constructed using extra data, including the PV power and efficiency. Then, each database variable is subjected to the logarithm function. The features are extracted and analyzed in the end. It may be challenging to tell the difference between sound operations and problematic ones when working with I-V curves in actual environmental situations.

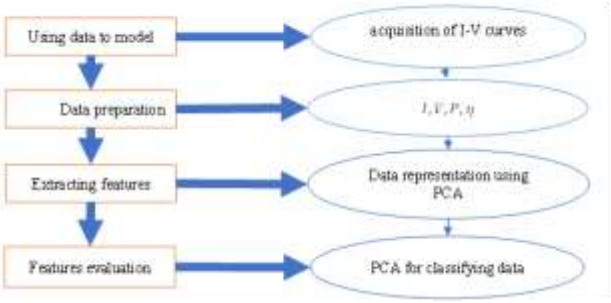

Figure 6. (FDC) algorithm's flowchart

IV. Formulation of the principal component analysis

Multiple variables for a statistical technique it's called principal component analysis (PCA) looks for the almost predominate dimensions in a multidimensional field of database-built configuration from a massive param of measurements acquired when various time. are produced by PCA. The initial major component which covers the primary the subspace is provided by the first l dominating eigenvectors of the data to covariance a matrix. them have related to the method eigenvalues with the largest l. The residual subspace is defined by the last pair of eigenvectors that are not kept (M-l). The eigenvectors are referred to as loading vectors in the domain of the representation with the biggest variations, and the projection of the data onto these loading vectors is referred to as principal component scores. Principal components (PCs) are the search directions, and each PC consists of a score and the loading vector component. Each PC's corresponding eigenvalue represents the proportion of the variance of the data it contains. beginning with the first PC, everyone PC is coordinated in the fitting that corresponds accordingly the data's greatest variation. Hence, the principal components are arranged from the most energetically charged to the lowest energetically How accurately the measurements gathered for fault identification are represented depends on how accurate the (PCA - model). The retained PCs are used in the above model to represent the data variability. the ordered column matrix of loading vectors in the eigenvalues' declining in rank is denoted by the letter P. To create the primary component scores, the original data is condensed and projected onto the fresh space spanned with P. The following formulas define the principal component scores' matrix T[NM]:

$$T[N \times M] = [(Xc)[N \times M] = [t1, \ldots, tk, \ldots, tM]]$$

4.1. Extraction of features and data prep processing, section

The variable selection is essential for the data to be effectively represented and differentiated. the finding of the Variables included the PV module's voltage, current, and power, to simulate the shading problem. Thanks to PCA, they were able to distinguish between good and bad data. However, in our instance, the use of these parameters has led to a sizable overlap in the territory covered by the major scores. This is due to the common voltage levels found in PV curves collected under shade faults as well as the difference in falling irradiance charged eigenvalue. According to stop criterion, the majority of the PCs in the principal subspace are connected to it, while the other PCs are connected to the residual subspace. Several halting criteria have been developed for this purpose. have been suggested in the literature, such as minimizing Variance of Concurrent Proportion of Overall Variance (CPV) and Variation in Reconstitution Error (VRE). Compared approaches to figure out how many PCs were using the most energy. PCA is utilized to analyze the data gathered during the process's healthy operating mode, and the model is then designed using the loading vectors as a reference. The implicit model can also be built utilizing the results or their statistical distributions. As new information is received, It is depicted in the auxiliary space. ((primary) or/and (residual)). Then, the difference from the point, of reference monitoring to measured and examined to determine whether a problem has occurred. Let's have a look at the initial data matrix X[NM] composed of M process variables, N observations are made., as stated by:

where $xj\ (j = 1,.N)$ is the jth variable.

First, it entails decreasing (unit variance) and concentrating (zero mean) the variables for each note k of $xj(\ j = \ 1,\ldots \mathrm{n}\ )$

$$(X_i)_c(k) = \frac{X(k)\ -(X_i)}{(\sigma_i)}$$

where (xj)c is the variable that has been reduced and centered, and (xj) and (j) are refer to value and standard between these measurements made during the like operational conditions (Figure 5). To have a fault diagnostic that is responsive to problem incidence and resilient to environmental changes, we have the following:

The PV voltage and power were normalized in proportion regard for PV efficiency using the log of function. The choice of those characteristics enables to make using of experimental measurements. acquired under operating settings with uncontrolled irradiance and little or no impact from the environment.

The training data

$$matrixX[(1010) \times (3)] = log\left[\frac{V}{\eta}, I, \frac{P}{\eta}\right]$$

formed of 1010 observations of three variables is eventually subjected to principal component analysis (Fig. 7), where P it's the power and η efficiency, respectively. It comprises of five 101*2 training observation submatrices.

For each pair of observations I, v) the efficiency is calculated and is represented as follows:

S is the area of the PV module that is being tested, and Equals

$$\eta = \frac{\mathrm{p}}{\mathrm{G_{mes}S}}\ 100\%$$

1515 samples make up the data set produced during the experimental experiments under both healthy and shaded settings. The training stage is carried out with 1010 samples as well as the initial two measurements Am and Bm from each test.

The primary responsibility of this stage is to build the PCA model using the learning data set. The test data set will be validated using this implicit model.

4.2. Features analysis in the training process, section

The eigenvalues and relative contributions are shown in Table 3. 99.99% of the information is retained on the first two Computers putting forth the training this data in the PCA subspace covered by PC1 and PC2, PC2 and PC3, and PC1 and PC3, respectively, resulted in the data dispersion displayed in Figs. 7 of 7a, of 7b, and 7c, respectively. The three key elements are included in the PCA are used to protect the data which enables the 3D depiction in Figure 7 of d. The shows in a subspace occupied by first two computers can be used to locate and identify the flaw. There are four classes visible: one sound class, denoted by the name c_1, and three flawed ones resulting from four incorrect setups, as indicated in Table 4. Indeed, shading configurations 2 and 3 depict the simultaneous activation of two bypass diodes. Between the sound class and the defective classes, there is an obvious distinction. The magnitude and position of the fault can be used to identify them. The confusion matrix shown in Table 5, it is used for the purpose of verifying the results.

Table 3. Eigenvalues with principal component contributions as a proportion

Principle component			
	(PC1)	(PC2)	(PC3)
Eigenvalue	1.990	1.007	3.08E-33
Variable %	66.46	33.55	1.03E-30

Table 4 . Classes in (PCA)

Test	Health state 1	Shading state 2	Shading state 3	Shading state 4
Class	C1	C2	C3	C4

4.3. Training step classification performance

The confusion matrix shown in Table 5 is used for the purpose of verifying the results. The columns of the table indicate the percentages of the observed part that proved to be affected by the subsequent signals in that category. The evaluation of error rates is for separating classes using the one-time cross-check method. Then, for each class in the PCA space, we compute the a priori coordinates of the gravity center in our instance, the mean Euclid.

Table 5. Identifying training data sets, use a confusion matrix

	Healthy state1	Faulty state 2	Faulty state 3	Faulty state 4
	C1%	C2%	C3%	C4%
Healthy state1	97.02	0	2.98	0
Faulty state 2	0	98.53	1.49	0
Faulty state 3	12.63	0	88.39	0
Faulty state 4	0	0	0	100

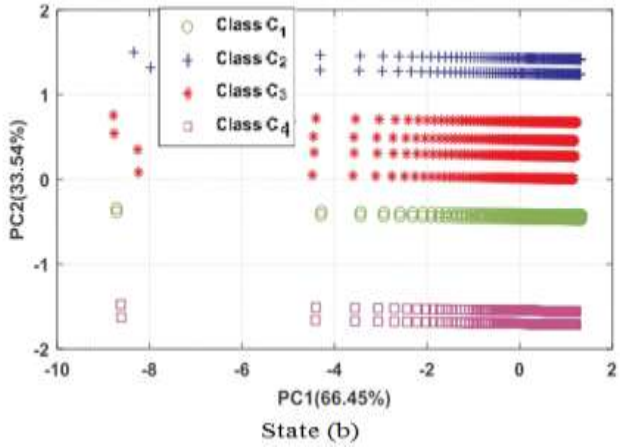

State (b)

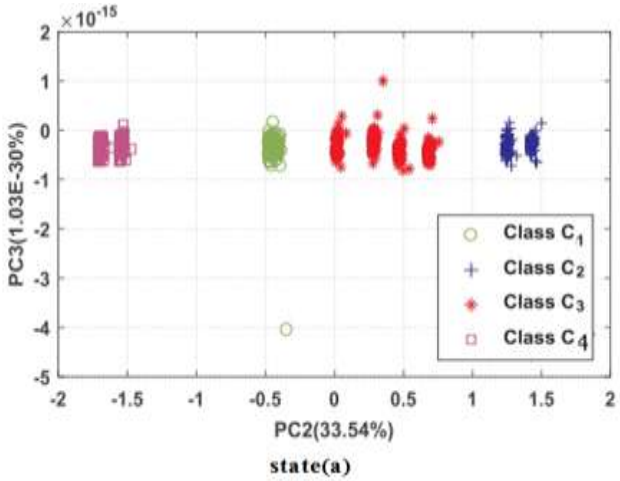

state(a)

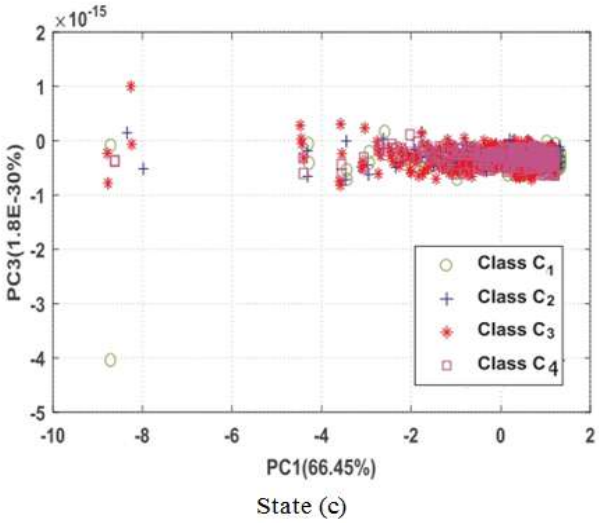

State (c)

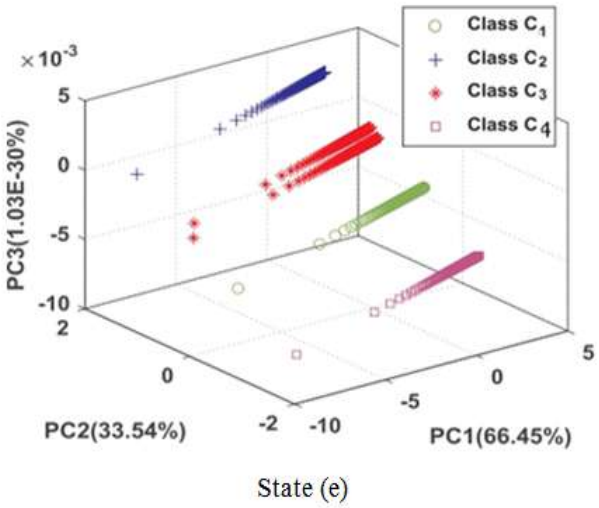

State (e)

Figure 7. Data dispersion

Conclusion

In this study, a data-driven Fault Detection and Classification (FDC) approach is presented for diagnosing shading defects in photovoltaic (PV) modules. Utilizing I &V curves under various conditions, the method applies Principal Component Analysis (PCA) to 66% of the training data, achieving a minimum 88.38% classification success rate for different fault scenarios. During validation with the remaining data, the success rate exceeds 98%. This cost-effective approach leverages standard PV current and voltage measurements, is unaffected by weather variations, and demonstrates PCA's effectiveness in diagnosing shading faults in PV systems.

Acknowledgements

We would like to express our gratitude to the Journal of Scientific Research at the University of Safx (Tunisia) for their generous support throughout this research endeavor. We extend our heartfelt thanks to Dr. Mohamed Boukattaya and Dr. Fatma Ben Salem for their invaluable assistance in preparing this paper. Their expertise and guidance have been instrumental in shaping the outcomes of this work. assistance in preparing this paper.

Declaration

- The authors declare that they have no known financial or non-financial competing interests in any material discussed in this paper.
- The authors declare that this article has not been published before and is not in the process of being published in any other journal.
- The authors confirmed that the paper was free of plagiarism.

References

[1] K. Ohdaira, M. Akitomi, Y. Chiba, A. “Potential-induced degradation of n-type front-emitter crystalline silicon photovoltaic modules — Comparison between indoor and outdoor test results”, Solar Energy Materials and Solar Cells, Vol. 249, 2023,112038 ISSN 0927-0248, https://doi.org/10.1016/j.solmat.2022.112038.

[2] B. -K. Kang, S. -T. Kim, S. -H. Bae and J. -W. Park, "Diagnosis of Output Power Lowering in a PV Array by Using the Kalman-Filter Algorithm," in IEEE Transactions on Energy Conversion, Vol. 27, no. 4, pp. 885-894, Dec. 2012, doi: 10.1109/TEC.2012.2217144. 8

[3] S. Fadhel, C. Delpha, D. Diallo, I. Bahri, A. Migan, M. Trabelsi, M.F. Mimouni, “PV shading fault detection and classification based on I-V curve using principal component analysis: Application to isolated PV system”, Solar Energy, Vol. 179, 2019, pp. 1-10, ISSN0038-092X https://doi.org/10.1016/j.solener.2018.12.04

[4] S. Bordihn, A. Fladung, J. Schlipf and M. Köntges, "Machine Learning Based Identification and Classification of Field-Operation Caused Solar Panel Failures Observed in Electroluminescence Images," in IEEE Journal of Photovoltaics, Vol. 12, no. 3, pp. 827-832, May 2022, doi: 10.1109/JPHOTOV.2022.3150725.

[5] A. Migan, C. Delpha, D. DialloI. I. Bahri, M. Trabelsi; M. Faouzi-Mimouni, "Data-driven approach for isolated PV shading fault diagnosis based on experimental I-V curves analysis," 2018 IEEE International Conference on Industrial Technology (ICIT), Lyon, France, 2018, pp. 927-932, doi: 10.1109/ICIT.2018.8352302.

[6] Koray Şener Parlak, Obtaining electrical characteristics of a PV module by FPGA based experimental system International Journal of hydrogen Energy, no. 58, 2020, pp. 3312833135, SSN0363199 , https ://doi.org/10.1016/j.ijhydene.2020.09 .113.

[7] Y. Zhu, W. Xiao, A comprehensive review of topologies for photovoltaic I–V curve tracer, Solar Energy, Vol. 196, 2020, pp. 346357, ISSN0038092X, https://doi.org/10.1016/j.solener.2019.12.020.

[8] M.de Jesus dos Santos Rodrigues, P. F. Torres, M. André Barros Galhardo, O. Andre Chase, W. Leão Monteiro, J. de Arimatéia Alves Vieira Filho, F. Menezes Mares, W. Negrão Macêdo, “A new methodology for the assessing of power losses in partially shaded SPV arrays,” Energy, Vol. 232, 2012, pp. 120938. ISSN 0360-5442 ,https://doi.org/10.1016/j.energy.2021.120938 .

[9] Q. Jia, Fault detection and recognition by hybrid nonnegative matrix factorizations, Chemometrics andIntelligentLaboratorySystems, Vol. 225, 2022, pp. 104553,ISSN01697439, https://doi.org/10.1016/j.chemolab.2022.104553.

[10] J J. Khanam , S. Y. Foo, "Neural Networks Technique for Maximum Power Point Tracking of Photovoltaic Array," SoutheastCon 2018, St. Petersburg, FL, USA, 2018, pp. 1-4, doi: 10.1109/SECON.2018.8479054.

[11] Fahmida, M. S. Alam, M. A. Hoque, "MATLAB Simscape Simulation of Solar Photovoltaic array fed BLDC Motor using Maximum Power Point Tracker," 2019 International Conference on Robotics,Electrical and Signal Processing Techniques (ICREST), Dhaka, Bangladesh, 2019, pp. 662-667, doi: 10.1109/ICREST.2019.8644339.

[12] H. S. Agha, Z. -u. Koreshi and M. B. Khan, "Artificial neural network based maximum power point tracking for solar photovoltaics," 2017 International Conference on Information and Communication Technologies (ICICT), Karachi, Pakistan, 2017, pp. 150-155, doi: 10.1109/ICICT.2017.8320180.

[13] V. K. Viswambaran, A. Ghani and E. Zhou, "Modelling and simulation of maximum power point tracking algorithms & review of MPPT techniques for PV applications," 2016 5th International Conference on Electronic Devices, Systems and Applications (ICEDSA), Ras Al Khaimah, United Arab Emirates, 2016, pp. 1-4, doi: 10.1109/ICEDSA.2016.7818506. 20).

[14] S. Zouirech, M. Zerouali, H. Elaissaoui, A. E. Ougli and B. Tidhaf, "Application of Various Classical and Intelligent MPPT Tracking Techniques for the Production of Energy through a Photovoltaic System," 2019 7th International Renewable and Sustainable Energy Conference (IRSEC), Agadir, Morocco, 2019, pp. 1-6, doi: 10.1109/IRSEC48032.2019.9078154.

[15] G. Abdel-rahman, N. H. Saad and A. A. -s. Abdel-fatah, "Performance Analysis of Fourth Order Buck Converter Based on Current Sensorless Maximum Power Point Tracking Technique for Photovoltaic Systems," 2018 Twentieth International Middle East Power Systems Conference (MEPCON), 2018.

[16] K. -Y. Chou, C. -S. Yang and Y. -P. Chen, "Deep Q-Network Based Global Maximum Power Point Tracking for Partially Shaded PV System," 2020 IEEE International Conference on Consumer Electronics - Taiwan (ICCE-Taiwan), 2020.

[17] P. Sahu, D. Verma, S. Nema, "Physical design and modelling of boost converter for maximum power point tracking in solar PV systems," 2016 International Conference on Electrical Power and Energy Systems (ICEPES), 2016.

[18] A. H. EL-Din, S. F. Mekhamer, H. M. EL-Helw, "Maximum power point tracking under partial shading condition using particle swarm optimization with DC-DC boost converter," 2018 53rd International Universities Power Engineering Conference (UPEC), 2018.

[19] J. Raju, B. T. Kumar, "Optimized maximum power point tracking technique for the simulation of photovoltaic system sourced for higher output power," 2017 International Conference on Innovations in Electrical, Electronics, Instrumentation and Media Technology (ICEEIMT), 2017.

[20] K. GB, Shivashankar, K. N. S. Kumar, "Optimum Power Point Tracking Technique for Standalone Solar Photovoltaic System," 2021 International Conference on Recent Trends on Electronics, Information, Communication & Technology (RTEICT), 2021.

[21] Sergiu Spataru, Dezso Sera, Tamas Kerekes, Remus Teodorescu, Diagnostic method for photovoltaic systems based on light I–V measurements, Solar Energy, Volume119,2015,Pages2944,ISSN0038092X,https://doi.org/10.1016/j.solener.2015.06.020 .

[22] M. Mao; Y. Zhao, S. Sun; L. Chang, Yu Cao, J.i Su, M.Sun, G. Zhang, "Quantitative analysis on economic impacts of installation at different sites on microgrids with multi-energy," 2012 3rd IEEE International Symposium on Power Electronics for Distributed Generation Systems (PEDG), Aalborg, Denmark, 2012, pp. 668-673, doi: 10.1109/PEDG.2012.6254074.

[23] M. Dhimish, V. Holmes, B. Mehrdadi, M. Dales, “Diagnostic method for photovoltaic systems based on six layer detection algorithm,” Electric Power Systems Research, Vol. 151, 2017, pp. 2639, ISSN03787796, https:// doi.org/ 10.1016/j.epsr.2017.05.024.

[24] Fadhel, S., Migan, A., Delpha, C., Diallo, D., Bahri, I., Trablesi, M., Mimouni, M.F., 2018. Data-Driven Approach for Isolated PV Shading Fault Diagnosis Based of Experimental I-V Curves Analysis. In: IEEE International Conference on Industrial Technology (ICIT), pp. 927–932.

[25] M.-Faouzi Harkat, G. Mourot, J. Ragot, “An improved PCA scheme for sensor FDI: Application to an air quality monitoring network,” Journal of Process Control, Vol. 16, no 6, 2006, pp. 625-634, ISSN 0959-1524,https: //doi.org/1 0.1016/j. jprocont .2005. 09.007.

[26] S. Fadhel, A. Migan, C. Delpha, D. Diallo, I. Bahri, M. Trablesi, M.F Mimouni. “Data-Driven Approach for Isolated PV Shading Fault Diagnosis Based on Experimental I-V Curves Analysis”. In: IEEE International Conference on Industrial Technology (ICIT), 2018, pp. 927–932.